

## REVIEW

View Article Online  
View Journal | View IssueCrossMark  
click for updatesCite this: *J. Mater. Chem. A*, 2015, 3,  
11700Received 12th January 2015  
Accepted 10th March 2015

DOI: 10.1039/c5ta00252d

www.rsc.org/MaterialsA

A review on mechanical exfoliation for the scalable  
production of grapheneMin Yi<sup>\*ab</sup> and Zhigang Shen<sup>\*a</sup>

Mass production and commercial availability are prerequisites for the viability and wide application of graphene. The exfoliation of graphite to give graphene is one of the most promising ways to achieve large-scale production at an extremely low cost. This review focuses on discussing different exfoliation techniques based on a common mechanical mechanism; because a deep understanding of the exfoliation mechanism can provide fruitful information on how to efficiently achieve high-quality graphene by optimizing exfoliation techniques. We highlight the recent progress on mechanical exfoliation for graphene production during the last decade. The emphasis is set on the widely used sonication method with the latest insight into sonication-induced defects, the newly explored ball milling method, the fluid dynamics method that has emerged in the last three years, and the innovative supercritical fluid method. We also give an outlook on how to achieve high-quality graphene efficiently using mechanical exfoliation techniques. We hope this review will point towards a rational direction for the scalable production of graphene.

## 1. Introduction

Graphene as a kind of two dimensional nanomaterial has attracted worldwide attention since its discovery in 2004,<sup>1–7</sup> and has become a hot topic mainly due to its outstanding properties and promising applications. As for its electric properties,

monolayer graphene is semi-metallic and its carriers are massless Dirac fermions whose dynamics are described by the Dirac equation.<sup>8</sup> Meanwhile, the electronic structure in single-layer graphene has band overlaps at two Dirac points in the first Brillouin zone, and the electron mobility at room temperature can reach  $2.5 \times 10^5 \text{ cm}^2 \text{ V}^{-1} \text{ s}^{-1}$ .<sup>9</sup> The maximum current density that monolayer graphene can bear is several million times larger than that in copper.<sup>10</sup> In terms of its mechanical properties, monolayer graphene has a Young's modulus of 0.5–1.0 TPa and a high intrinsic strength of  $\sim 130 \text{ GPa}$ ,<sup>11</sup> which approaches the predicated theoretical value.<sup>12</sup> Furthermore, monolayer graphene has a high thermal conductivity of  $\sim 3000$

<sup>a</sup>Beijing Key Laboratory for Powder Technology Research and Development, Beijing University of Aeronautics and Astronautics, Beijing 100191, China. E-mail: yimin@buaa.edu.cn; shenzhg@buaa.edu.cn; Fax: +86 10-82338794; Tel: +86 10-82317516

<sup>b</sup>Institute of Materials Science, Technische Universität Darmstadt, Darmstadt 64287, Germany



Min Yi was born in Hunan, China in 1987. He received his bachelors degree in engineering mechanics from Beijing University of Aeronautics and Astronautics (Beihang University, BUAA) in 2010. Then he pursued his PhD degree in the group of Prof. Zhigang Shen at BUAA. Presently, he is a visiting scholar at the Institute of Materials Science, TU Darmstadt, Germany. His current research

interests are focused on the production of graphene and its analogues and their relevant applications, and mechanics of functional materials.



Zhigang Shen is a full professor at Beijing University of Aeronautics and Astronautics (Beihang University, BUAA) and is the director of the Beijing Key Laboratory for Powder Technology Research and Development. He received his PhD degree in aerodynamics from BUAA in 1989. Since then, he has worked at BUAA as a professor. His research interests include the design, mechanical

synthesis and chemical synthesis of powders, functional nanoparticles, graphene and graphene analogues, and their applications in lubrication, energy, and space protection.

W mK<sup>-1</sup>,<sup>13,14</sup> extremely high resistance to gas permeation,<sup>15</sup> a high transmittance of ~97.7%,<sup>16</sup> *etc.* These unique properties make graphene suitable for many applications such as electronic devices, photonic devices, advanced composites, paint, coatings, energy storage, sensors, metrology, biology, *etc.*<sup>6</sup> These outstanding properties and promising applications have stimulated the production of graphene.

Up to now, a large number of methods have been proposed to produce graphene. These methods can be categorized into two major classes, *i.e.* bottom-up methods and top-down methods. The former depends on the chemical reaction of molecular building blocks to form covalently linked 2D networks. The latter relies on the exfoliation of graphite. Bottom-up techniques, such as chemical vapor deposition and epitaxial growth, can yield high-quality graphene with a small number of defects.<sup>17–25</sup> The resultant graphene is a good candidate for electronic devices. However, these substrate-based techniques suffer from a limited scale and expensive production, and cannot meet the requirements of macroscopic quantities of graphene. Large-scale production of graphene at a low cost has been demonstrated to be possible using top-down techniques, whereby graphene is produced through the direct exfoliation of graphite in the liquid phase.<sup>26–32</sup>

This review will discuss the available routes for the large-scale production of graphene in terms of the exfoliation of graphite. Note that several reviews have already summarized the art-to-date progress of the liquid-phase exfoliation of graphite or graphite oxide to give graphene or graphene oxide.<sup>26–28,33–35</sup> From a different perspective, this review will focus on the common mechanical mechanism involved in the exfoliation techniques; because the exfoliation mechanism is an important factor, which needs deep understanding and should provide fruitful information on how to efficiently achieve high-quality graphene by optimizing exfoliation techniques. With this consideration, we will not discuss exfoliation media, such as suitable organic solvents,<sup>29,36</sup> mixed solvents,<sup>37,38</sup> surfactant/water solutions,<sup>39–42</sup> aromatic solvents,<sup>43</sup> ionic liquids,<sup>44,45</sup> *etc.*, in which the exfoliation occurs. We will also not discuss the difference between the exfoliation-mediated preparation of graphene and graphene oxide; because the involved exfoliation mechanics are almost the same. In contrast, we will concentrate on the exfoliation techniques themselves in terms of the mechanical exfoliation mechanism.

In this review, we aim to provide an overview of recent developments in mechanical exfoliation techniques for producing graphene. This review includes not only the widely used sonication method, but also the ball milling and fluid dynamics methods which have emerged during the last three years. Firstly, we will elucidate the mechanical mechanism for exfoliation. In this way, the different exfoliation techniques are united by their common mechanism. Then we will thoroughly discuss mechanical exfoliation techniques, such as the original micromechanical cleavage, the most widely used sonication method, the newly explored ball milling method, the recently emerged fluid dynamics method, the innovative supercritical fluid method, *etc.* Finally, we will give conclusions and an outlook.

## 2. Mechanical exfoliation mechanism

Within the top-bottom concept, graphene is prepared by exfoliating graphite. In this process, the ideal case is that graphene can be peeled from the bulk graphite layer by layer. The resistance to overcome is the van der Waals attraction between adjacent graphene flakes. How to overcome the attraction force, peel the layer, and then achieve graphene is more or less a mechanical issue. In general, there are two kinds of mechanical routes to exfoliate graphite into graphene flakes, *i.e.* normal force and lateral force. One can exert normal force to overcome the van der Waals attraction when peeling two graphite layers apart, such as micromechanical cleavage by Scotch tape.<sup>1,2</sup> Through graphite self-lubricating ability in the lateral direction, one can also exert lateral force to promote the relative motion between two graphite layers. These two mechanical routes are illustrated in Fig. 1. It should be noted that for all of the reported exfoliation techniques up to now, these two mechanical routes are prerequisites for the production of graphene. It can be anticipated that the controlled exfoliation of graphite to give high-quality graphene with a high efficiency is feasible by tailoring these two mechanical routes.

Another auxiliary route is the fragmentation effect during exfoliation, as shown in Fig. 1. The force generated by the exfoliation technique can also fragment large graphite particles or graphene layers into smaller ones. This fragmentation effect has double-faced tactics. On the one hand, it can reduce the lateral size of graphene. This is not desirable for achieving large-area graphene. On the other hand, it facilitates exfoliation, because smaller graphite flakes are easier to exfoliate than larger ones because of the smaller collective van der Waals interaction forces between the layers in smaller graphite flakes. In the following sections, in terms of the above two mechanical routes, several mechanical exfoliation techniques are reviewed.

## 3. Mechanical exfoliation techniques

### 3.1 Micromechanical cleavage

Both the birth of the first graphene flake in the real world and the Nobel prize for Physics in 2010 are attributed to the micromechanical cleavage of HOPG (Highly Ordered Pyrolytic Graphite) in 2004.<sup>1,2,46</sup> The general idea of this method is the cleavage of graphene layers from the bulk HOPG surface. The

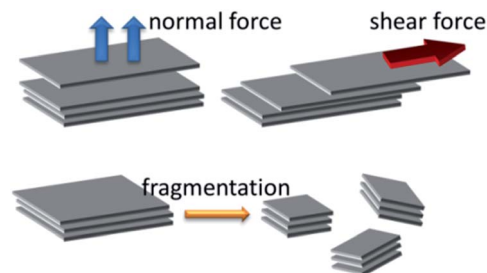


Fig. 1 Two kinds of mechanical routes for exfoliating graphite into graphene flakes and the auxiliary route for fragmentation.

procedure is presented in Fig. 2. The exfoliation mechanics of this method are that the Scotch tape is applied to the HOPG surface and thus exerts a normal force. If one takes great pains to repeat this normal force numerous times, the graphitic layer becomes thinner and thinner and finally it will become single-layer graphene. This is exactly what the winners of the 2010 Nobel Physics prize did in 2004. The exfoliation mechanics are dominated by a normal force. This method can be used to prepare high-quality and large-area graphene flakes. Based on the graphene samples prepared by this method, many outstanding properties of graphene have been discovered. However, this method is extremely labour-intensive and time-consuming. It is limited to laboratory research and seems impossible to scale up for industrial production.

In order to save labour and enhance the efficiency, Jayasena *et al.* devised a lathe-like experimental setup to cleave HOPG samples for generating graphene flakes,<sup>47</sup> as shown in Fig. 3. The HOPG sample is trimmed into a pyramid shape and then embedded into epoxy (Fig. 3a and b). The tool for cleaving HOPG is an ultrasharp single crystal diamond wedge. The diamond wedge is mounted onto an ultrasonic oscillation system and is aligned carefully with respect to the HOPG mount (Fig. 3c). When the ultrasharp wedge is held fixed and the work material is fed slowly downwards towards the wedge, lathe-like behaviour happens and the lathed products sliding off the diamond wedge surface are cleaved graphite flakes. This method is lathe-like and can be scaled up to available lathe techniques, but the obtained thin flakes have a thickness of tens of nanometers. Further precise control of the diamond wedge is required for achieving high-quality graphene.

Another micromechanical technique inspired by the “Scotch tape” method uses a three-roll mill machine with a polymer adhesive.<sup>48</sup> A preparation process using a three-roll mill is illustrated in Fig. 4. Polyvinyl chloride (PVC) dissolved in dioctyl phthalate (DOP) is used as the adhesive, which plays a similar role to Scotch tape in the original micromechanical cleavage. The dispersion and exfoliation happen in the adhesive. As shown in Fig. 4, the moving rolls can drive the graphite flakes to run in an inverted S curve from the feed roll to the apron roll, then turn back towards the feed roll, leading to continuous

exfoliation. Though the three-roll mill machine is a very common industrial technique used in the rubber industry and is easily available, the complete removal of residual PVC and DOP to obtain graphene is not easy and brings about additional complexity.

### 3.2 Sonication

Sonication assisted liquid-phase exfoliation of graphite to give graphene has made the large-scale production of graphene possible. Following their experience in dispersing carbon nanotubes by sonication, Coleman's group first reported the high-yield production of graphene by the sonication assisted liquid-phase exfoliation of graphite in 2008.<sup>29</sup> In their work, graphite powder was dispersed in specific organic solvents, such as *N,N*-dimethylformamide (DMF) and *N*-methylpyrrolidone (NMP), followed by sonication and centrifugation. Then graphene dispersion was obtained, as shown in Fig. 5a. The contrast between the scanning electron microscopy (SEM) image of the initial graphite flakes in Fig. 5b and the transmission electron microscopy (TEM) image in Fig. 5c show the exfoliation degree. The prepared graphene was evidenced by different characterizations such as TEM (Fig. 5c), atomic force microscopy (AFM) (Fig. 5e), *etc.* The number fraction of mono-layer graphene can be estimated as 28% (Fig. 5d). This method is extremely intriguing and opens a whole new vista for the large-scale and low-cost production of graphene. A benefit of this method is that producing graphene seems very easy. The most shortcoming issue is the extremely low graphene concentration ( $\sim 0.01 \text{ mg mL}^{-1}$ ), which is far from practical application. After this work, based on the same idea, a great many researchers have contributed to achieving high-concentration graphene by prolonging the sonication time, increasing the initial graphite concentration, adding surfactants and polymers, solvent exchange methods, mixing solvents, *etc.*<sup>37–45,49–63</sup>

It has been demonstrated that such a kind of liquid-phase exfoliation of graphite is attributed to the small net energetic cost during the exfoliation process.<sup>29</sup> This energy balance for the graphene and solvent system can be expressed as the enthalpy of mixing per unit volume, *i.e.*

$$\frac{\Delta H_{\text{mix}}}{V_{\text{mix}}} \approx \frac{2}{T_{\text{flake}}} (\delta_{\text{G}} - \delta_{\text{sol}})^2 \phi$$

in which  $T_{\text{flake}}$  is the thickness of a graphene flake,  $\phi$  is the graphene volume fraction, and  $\delta_i$  is the square root of the surface energy of phase *i* (*i* denotes graphene or solvent) which is defined as the energy per unit area required to overcome the van der Waals forces when peeling two sheets apart. It is obvious that when the graphene and solvent surface energies are close, the mixing enthalpy will be smaller and the exfoliation occurs more easily. Therefore, the surface energy of a solvent is imperative for such a kind of exfoliation. By using a range of solvents with different surface energies and measuring the corresponding concentration of the resultant graphene dispersions, the optimal surface energy of the solvents can be roughly estimated, as shown in Fig. 5g. The good solvents tend

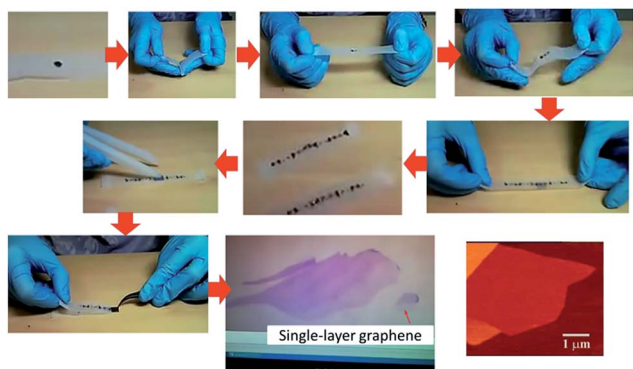


Fig. 2 An illustrative procedure of the Scotch-tape based micro-mechanical cleavage of HOPG.



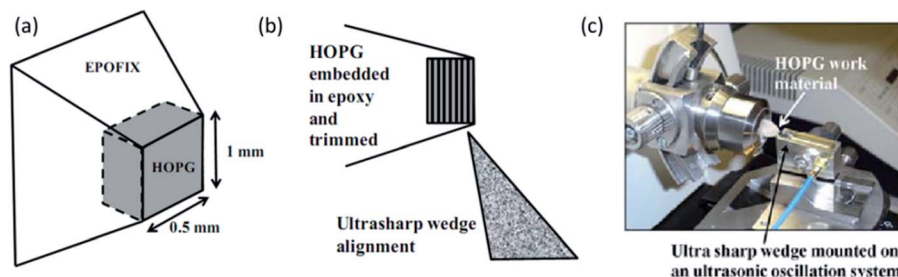


Fig. 3 (a) HOPG mounted in epofix and trimmed to a pyramid shape. (b) Setup showing the wedge alignment with HOPG layers. (c) Actual experimental setup. Reproduced with permission from ref. 47. Copyright 2011 Springer.

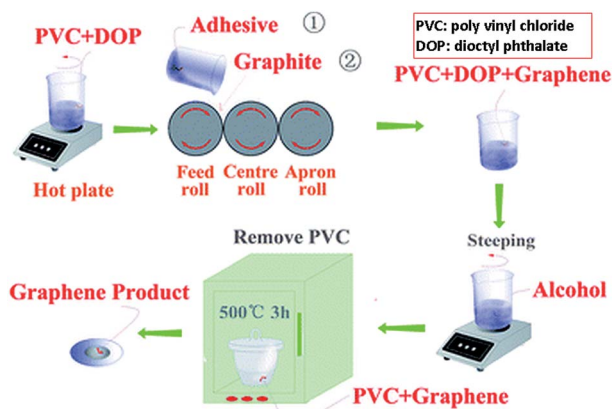


Fig. 4 Schematic illustration for exfoliating natural graphite using a three-roll mill. Reproduced with permission from ref. 48. Copyright 2012 The Royal Society of Chemistry.

to have a surface energy of  $70\text{--}80\text{ mJ m}^{-2}$ , or a surface tension of  $40\text{--}50\text{ mJ m}^{-2}$ . However, these results are obtained at room temperature and short sonication times. If the temperature is elevated, the surface energy and the surface tension will be changed. If the sonication time is long or sonication is intensive, the solvents would suffer from degradation and their properties will also be changed. These may make the large-scale production of graphene by sonication fail. Therefore, in these conditions, the above-mentioned model should be modified. Actually, Lin *et al.*<sup>64</sup> has recently noticed this. When studying the effect of solvent surface energy on the solvothermal deoxidation of graphene oxide, they found that the solvent surface energy should be tuned with respect to the temperature. They also established a temperature-dependent model of surface energy engineering for the large-scale production of graphene and highly reduced graphene oxide.

There have been two reviews concerning the details of the recent work on the sonication assisted production of graphene.<sup>30,65</sup> In this review, we will not present these details, and will only focus on the exfoliation mechanics and the involved problems. In the sonication method, the exfoliation mechanics originate from the liquid cavitation, as illustrated in Fig. 6. The cavitation-induced bubbles distribute around the graphite flakes. When these bubbles collapse, micro-jets and shock waves will act on the graphite surfaces instantly, resulting in

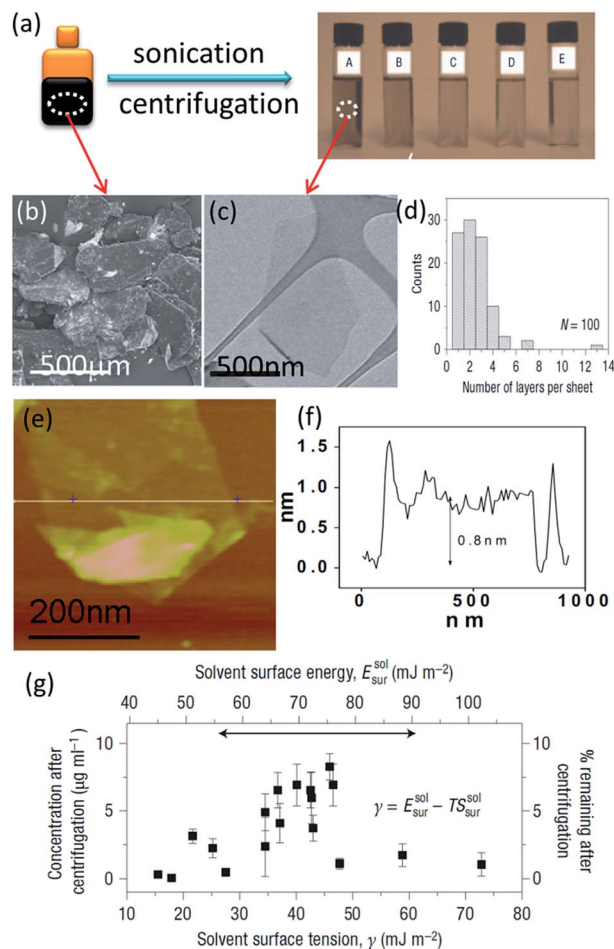


Fig. 5 (a) Sonication of graphite dispersion giving graphene dispersion. (b) SEM image of the initial graphite flakes. (c) TEM image of the exfoliated graphene. (d) Histogram of the layer number. (e) AMF image and (f) the corresponding height profile. (g) Graphite concentration measured after centrifugation for a range of solvents plotted versus solvent surface tension and surface energy. Reproduced with permission from ref. 29. Copyright 2008 Nature Publishing Group.

compressive stress waves which propagate throughout the graphite body. According to the theory of stress waves, once the compressive wave spreads to the free interface of graphite, a tensile stress wave will be reflected back to the body. As such, collapses of numerous micro-bubbles will lead to intensive

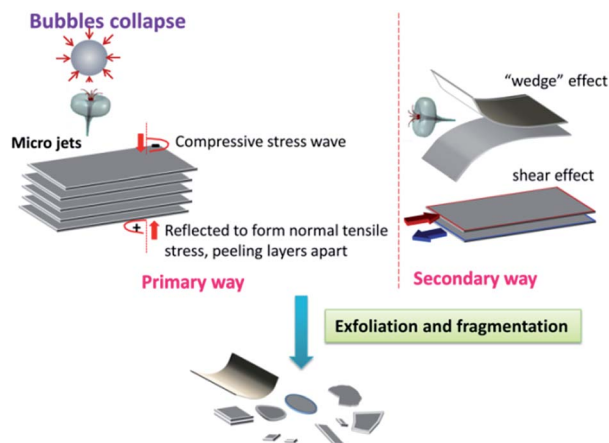


Fig. 6 Illustration of the mechanical mechanism for exfoliation via sonication.

tensile stress in the graphite flakes; just as intensive ‘sucking discs’ exfoliate the flakes. In addition, a secondary process is possible in that the unbalanced lateral compressive stress can also separate two adjacent flakes by a shear effect. Also, the micro-jets may split the graphite flakes just as a wedge is driven into the interlayer. In a word, it is the tensile stress that effectively exfoliates graphite into graphene flakes, resulting in a normal force dominated way.

The sonication technique has been deemed vitally successful in the liquid-phase exfoliation of graphene. However, recently there have also been several publications which have focused on the shortcomings of sonication.

Firstly, it has been demonstrated recently that the graphene prepared by sonication has many more defects than expected.<sup>66–69</sup> This shortcoming is intrinsically attributed to the sonication-induced cavitation. Although cavitation is favourable for exfoliation, it is a relatively harsh process which can produce a high local temperature ( $\sim$ several thousand K), extreme pressure ( $\sim$ several thousand atm), and rapid heating/cooling rates ( $\sim$ several billion  $\text{K s}^{-1}$ ).<sup>70–72</sup> These harsh conditions involved in cavitation could result in damage to the graphene. Actually, Polyakova *et al.*,<sup>69</sup> who were the first to have performed an in-depth spectroscopic study on graphene prepared by sonication, demonstrated that graphene made by sonication processes may be inferior, as shown in Fig. 7. By using X-ray photoelectron spectroscopy (XPS), they found that the sonication-produced graphene flakes contain a lot of oxygen which was only found in graphene oxide, as shown in Fig. 7f and g. They also for the first time visualized the defects in sonication-produced graphene flakes by scanning tunneling microscopy (STM), as shown in Fig. 7a–d. Subsequently, Skaltsas *et al.*<sup>67</sup> investigated the effect of sonication time and/or power on the oxygen content in exfoliated graphene. They also evidenced that sonication can cause defects and induce oxygen functional groups in the form of carboxylic acids and ethers/epoxides onto the graphene lattice, as schematized in Fig. 7h. In contrast, Yi *et al.*<sup>68</sup> dispersed liquid-exfoliated graphene in water and found that the oxygen-containing groups were mainly

attached to the edge and “hole-like” defects in the basal plane, as shown in Fig. 8a. In more detail, Bracamonte *et al.*<sup>66</sup> recently reported that defect localization strongly depends on the sonication time. Defects are located mainly at the layer edge for short sonication times, while they will build up in the basal plane for sonication times above two hours, as shown in Fig. 8b. They also suggested that the basal plane defects are not vacancies, nor substitutional impurities or  $\text{sp}^3$ -like but rather topological defects. In contrast to the widely addressed issue that liquid-phase exfoliated graphene by sonication is believed to be disorder-free or defect-free,<sup>26,27,29,39,40,50,52,54</sup> these results indicate the existence of defects on both the edges and basal planes. These defects should be intrinsically due to the sonication-induced cavitation. Also, they should depend on the solvents, ambient conditions, sonication time, sonication power, *etc.* The improvement of sonication as a strategy toward the exfoliation of really defect-free graphene is highly recommended. These issues still remain as an interesting subject for study.

Secondly, the distribution and intensity of the sonication-induced cavitation are highly dependent on the vessel size and shape which often induce localized cavitation pictures.<sup>74–77</sup> Thus, the vessel size and shape are bound to affect the sonication-assisted production processes of graphene. It should be mentioned that the lack of details about the geometry and position of the vessels in publications hinders the comparison of experimental results such as graphene concentration and production efficiency between each study. In fact, some researchers have noted that the final graphene concentration is largely affected by vessel geometry and dispersion volume.<sup>44,52</sup> In more detail, with the combination of simulation and experiment, it is found that the vessel diameter and liquid height can affect both cavitation volume and cavitation volume fraction, thus influencing graphene concentration (Fig. 9), graphene yield, production efficiency, *etc.*<sup>73</sup> Recently, Han *et al.*<sup>78</sup> adjusted the sonication probe depth to the liquid surface to generate less energetic cavitation for exfoliated transition metal dichalcogenide nanosheets and less defective, large graphene oxide nanosheets. But the production of pristine graphene was not reported. For the mass production of graphene for industrial applications, the geometry of sonication vessels should be mandatorily changed and redesigned when taking the set-up from laboratory to industry. The knowledge on the scale-up of the sonication vessels is indispensable. Meanwhile, other parameters such as sonication frequency, sonication power, sonication source distribution, temperature, *etc.* should also be considered. These issues in terms of the scale-up from laboratory to industry are worth deeply investigating.

The last minor issue to be remarked upon is the efficiency of sonication in the liquid-phase exfoliation of graphene. Both in an ultrasonic bath or with an ultrasonic probe, if the position of the ultrasonic vibration source is fixed, the cavitation field in the liquid is almost static. This is not favourable for efficient exfoliation, because graphite flakes will be exfoliated many times in the region of high cavitation intensity while may remain intact in the region of low cavitation intensity. This is really the case, especially when the initial graphite concentration is high and a large quantity of

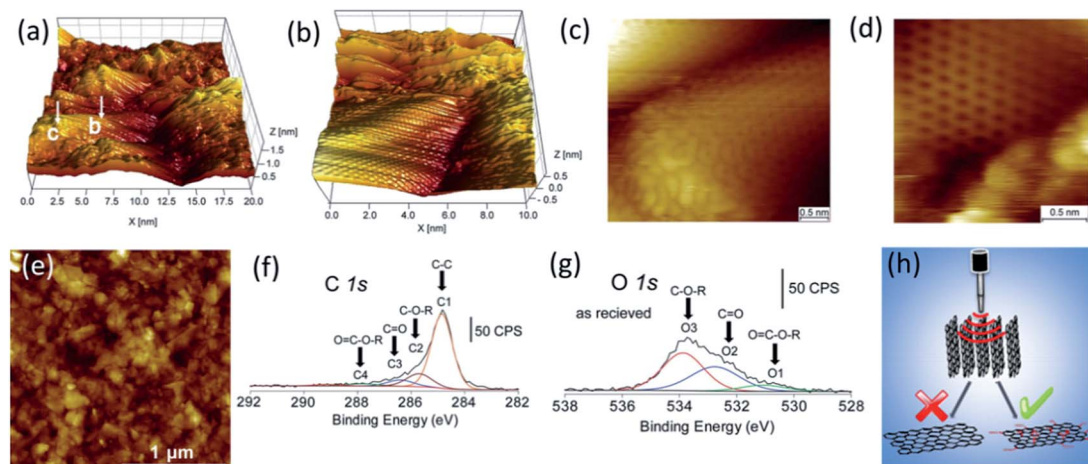


Fig. 7 (a) 3D STM image of a  $20 \times 20 \text{ nm}^2$  area of the graphene film. (b) 3D STM image of the region around the arrow b in (a). (c) STM image of the superstructure near an isolated defect around the arrow c in (a). (d) High-resolution STM image of a border between "perfect" and "functionalized" regions. (e) Typical AFM image of a graphene film prepared by sonication-assisted dispersion in DMF. (f) C 1s peaks and (g) O 1s peaks in the XPS spectra of the graphene film in (e). (h) Illustration of sonication causing defects and oxygen functional groups in the graphene lattice. Reproduced with permission from ref. 67 and 69. Copyright 2011 and 2013 American Chemical Society.

graphite flakes which settle down to the bottom still remain unexfoliated. For this consideration, a moving cavitation field or sonication combined with stirring should be helpful for efficient exfoliation.

### 3.3 Ball milling

Besides the sonication-based exfoliation method which is a normal-force-dominated way, shear force can also be utilized to laterally exfoliate graphite into graphene flakes, as schematized in Fig. 1. Ball milling, a common technique in the powder production industry, is a good candidate for generating shear force. The mechanical mechanism of ball milling in exfoliating graphene can be illustrated in Fig. 10. In most ball milling apparatus, there are two possible ways responsible for the exfoliation and fragmentation effects. The primary one is the shear force, which is thought to be an excellent mechanical route for exfoliation. This way is highly desired for achieving

large-sized graphene flakes. The secondary one is the collisions or vertical impacts applied by the balls during rolling actions. In this way, large flakes can fragment into small ones, and sometimes even destroy the crystalline nature of structures to form amorphous or non-equilibrium phases. Therefore, it is expected that to attain high-quality and large-sized graphene, the secondary effect should be minimized.

**3.3.1 Wet ball milling.** Initially, ball milling was adopted to reduce the size of graphite, and it was found that graphitic flakes with a thickness down to 10 nm could be obtained.<sup>81–83</sup> But this milling scheme was not further continued to obtain graphene. Until 2010, following the same idea as the sonication-based liquid-phase exfoliation of graphene, Knieke *et al.*<sup>84</sup> and Zhao *et al.*<sup>85,86</sup> modified the milling technique to produce graphene. After this initiative, the research on producing graphene by ball milling flourished. Generally, two types of ball milling techniques, *i.e.* planetary ball mills<sup>79,85–96</sup> and stirred media

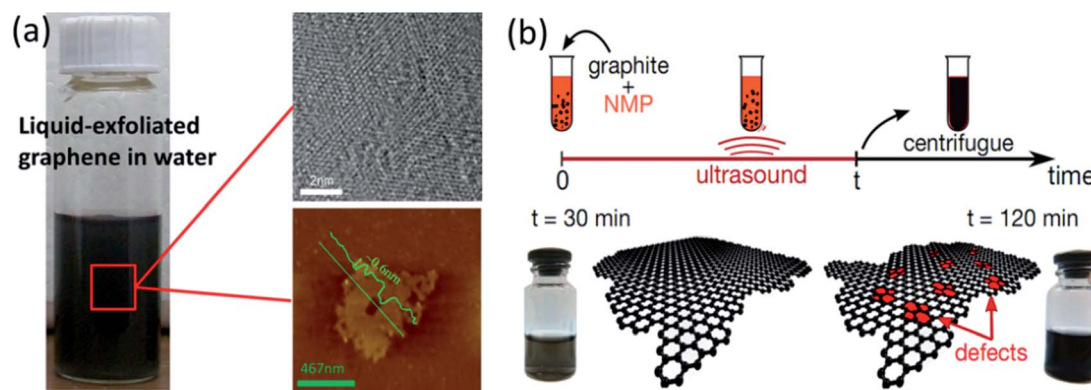


Fig. 8 (a) Dispersion of liquid-exfoliated graphene in water due to the reduction of flake size, "hole-like" defects and thus the enhanced edge effects. (b) Defect localization depends on the sonication time. Reproduced with permission from ref. 66 and 68. Copyright 2013 The Royal Society of Chemistry and 2014 American Chemical Society.



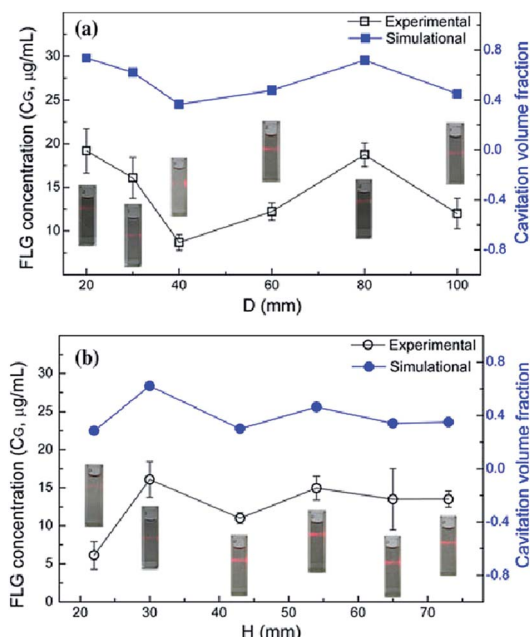


Fig. 9 Graphene concentration  $C_G$  and cavitation volume fraction calculated from finite element simulation results as a function of vessel diameter  $D$  (a) and vessel height  $H$  (b). Reproduced with permission from ref. 73. Copyright 2012 Springer.

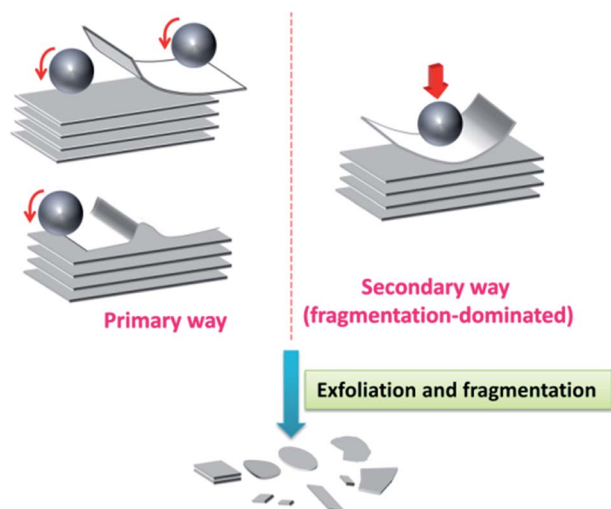


Fig. 10 Illustration of the mechanical mechanism for exfoliation via ball milling.

mills,<sup>80,84</sup> are widely used. Recently, planetary ball milling with graphite in the wet state has been investigated continuously for graphene production. By dispersing graphite in “good” solvents which have a matched surface energy for overcoming the van der Waals forces of adjacent graphene flakes, such as DMF, NMP, tetramethylurea, *etc.*, Zhao *et al.*<sup>85,86</sup> used a planetary mill for wet ball milling to get graphene. This scheme depends on long-time milling ( $\sim 30$  h) and the rotating tray should be controlled at a low speed ( $\sim 300$  rpm) to ensure that the shear stress is dominant. Aqueous solutions of surfactant (*e.g.* sodium

dodecyl sulfate) can also serve as the wet medium for ball milling graphite. But the exfoliation degree is relatively low and subsequent sonication is required.<sup>88</sup> In order to increase the exfoliation degree and efficiency, Aparna *et al.* combined high-energy ball milling with strong aqueous exfoliants. They dispersed graphite into a mixture of 1-pyrene carboxylic acid and methanol, and found that much faster exfoliation was achieved when compared to the usage of DMF.<sup>89</sup> Similar to this combined scheme, Rio-Castillo *et al.* recently used an exfoliating agent (melamine) for the intercalation of graphite layers, and found that adding a small amount of solvent during the ball milling process can enhance the intercalation and promote exceptional exfoliation. In this way, they demonstrated the successful ball milling exfoliation of carbon nanofibres into monolayer graphene,<sup>79</sup> as schematized in Fig. 11.

It should be noted that the above work is all about planetary ball milling. The advantage of planetary ball milling is that its high energy is favourable for combined functionalization and exfoliation, while a drawback is the long processing time (several ten hours) and/or requirement of sonication-assisted post-dispersing steps. In contrast to planetary ball mills, Knieke *et al.*<sup>84</sup> and Damm *et al.*<sup>80</sup> used wet stirred media mills which operate with much smaller grinding media and allow a better temperature control during the processing. From a technical viewpoint, they optimized the milling tool, delamination media size, and stirrer rotation speed.<sup>80</sup> By using a shaking plate as a milling tool, they found that the dispersed carbon concentration increased with a growing  $\text{ZrO}_2$  bead size, whereas the few-layer graphene (FLG) concentration and the percentage of FLG reached a maximum at a  $\text{ZrO}_2$  bead size of  $100\ \mu\text{m}$ , as shown in Fig. 12a. In contrast, Fig. 12b gives the stirrer tip speed dependent results for the stirred media mill. The dispersed carbon concentration and the FLG concentration are remarkable higher than those for the shaking plate, see Fig. 12a and b. This result indicates that the stirred media mill is more efficient than the shaking plate.<sup>80</sup>

**3.3.2 Dry ball milling.** Besides wet milling, dry milling can also be used for producing graphene. By ball milling a mixture of graphite and chemically inert water-soluble inorganic salts, a shifting of the layers in graphite can be achieved. Subsequent water washing and/or sonication of the milling products can lead to graphene powders,<sup>92,95</sup> as illustrated in Fig. 13. When

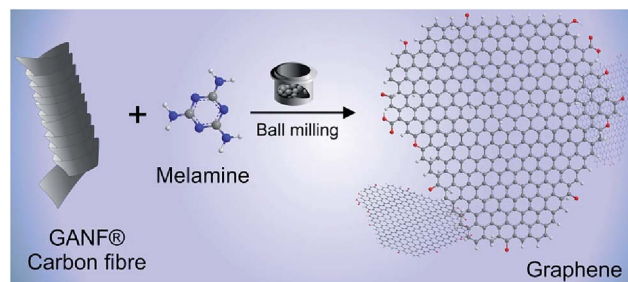


Fig. 11 Ball milling exfoliation of carbon nanofibres into graphene by using melamine as an exfoliating agent. Reproduced with permission from ref. 79. Copyright 2014 Springer.

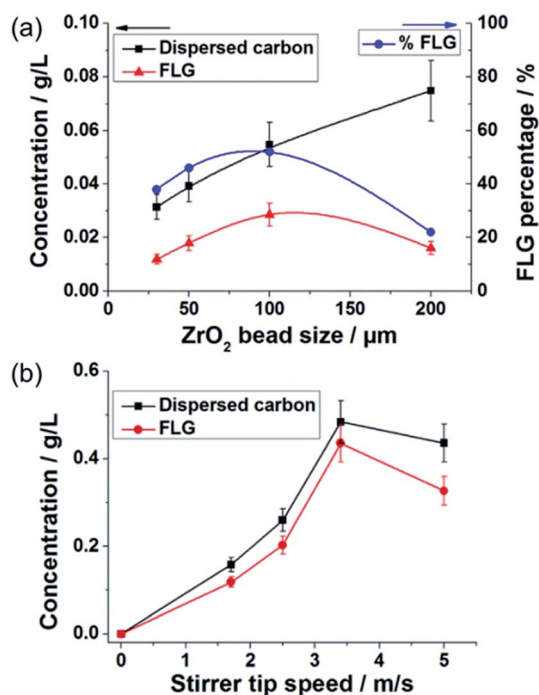


Fig. 12 (a) Left axis: dispersed carbon concentration (squares) and (FLG) concentration (triangles), right axis: percentage of FLG in the product (circles), obtained after 1 h of processing using a shaking plate disperser as a function of the diameter of the ZrO<sub>2</sub> beads. (b) Dispersed carbon concentration (squares) and FLG concentration (circles) obtained after 1 h of delamination using a stirred media mill and 100 μm ZrO<sub>2</sub> beads as delamination media as a function of the stirrer tip speed. Reproduced with permission from ref. 80. Copyright 2014 Elsevier.

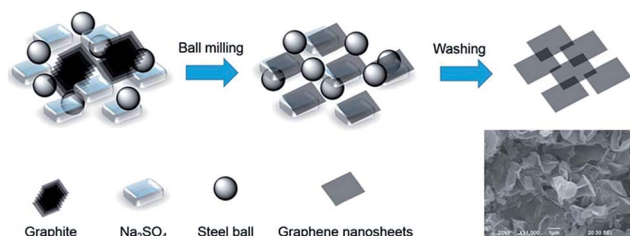


Fig. 13 Schematic of the soluble salt-assisted ball milled route to graphene nanosheet powder. The inset is the SEM image in the case that the weight ratio of Na<sub>2</sub>SO<sub>4</sub> powder to graphite powder is 600 : 1. Reproduced with permission from ref. 95. Copyright 2014 The Royal Society of Chemistry.

combined functionalization and exfoliation is required, dry milling also shows practical advantages. By using the similar electro-negativities of sulfur and graphene and thus the large attraction between them, Lin *et al.* ball milled a mixture of chemically modified graphite and elemental sulfur to get graphene/sulfur composites in which the sulfur molecules are anchored onto graphene sheets (Fig. 14).<sup>96</sup> Depending on a hydrogen-bonding network for the formation of multipoint interactions with the surface of graphene, Leon *et al.* used a ball milling treatment to exfoliate graphite through interactions

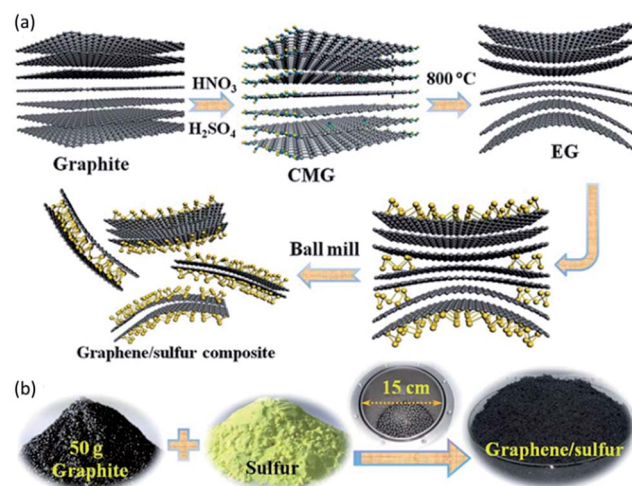


Fig. 14 (a) Illustration of the evolution process from graphite to graphene. (b) Mass production of graphene-sulfur composites prepared by ball milling graphite flakes with sulfur. Reproduced with permission from ref. 96. Copyright 2013 The Royal Society of Chemistry.

with commercially available melamine in the solid state.<sup>94</sup> In contrast to these methods which suffer from the basal plane functionalization of graphene, Jeon *et al.* put forward an edge functionalization route for the scalable production of graphene by ball milling.<sup>87,90,91</sup> They dry milled graphite in the presence of hydrogen, carbon dioxide (Fig. 15), sulfur trioxide, or a carbon dioxide/sulfur trioxide mixture. Upon exposure to air moisture, the resultant hydrogen-, carboxylic acid-, sulfonic acid-, and carboxylic acid/sulfonic acid functionalized graphene flakes are obtained. By ball milling the pristine graphite flakes in Fig. 15e for 48 h in the presence of dry ice, homogenous but much smaller edge-carboxylated graphite grains (100–500 nm) can be obtained (Fig. 15f). The edge-carboxylated graphite is highly dispersible in various solvents and can self-exfoliate into mono- and few-layer graphene nanosheets, as shown in the TEM images in Fig. 15g and h. These examples of edge-selectively functionalized graphene proved to be of a high quality.

Though the ball milling technique is thought of as an intriguing method for the large-scale production of graphene, the defects induced by the high-energy collision of grinding media are less clear. Since collisions among the grinding media cannot be prevented during the milling process, fragmentation and defects are unavoidable. This is really a double-edged sword. On the one hand, it can be used to functionalize graphene and favour efficient exfoliation. On the other hand, it will reduce the graphene size and introduce defects, especially basal defects. The choice of ball milling should depend on the prescribed requirement of different-level graphene.

### 3.4 Fluid dynamics

Besides the above discussed sonication and ball milling, a fluid dynamics method for producing graphene recently arose. Within the fluid dynamics method, graphite flakes can move with the liquid and can thus be exfoliated repeatedly at different positions. This feature is intrinsically different from that of



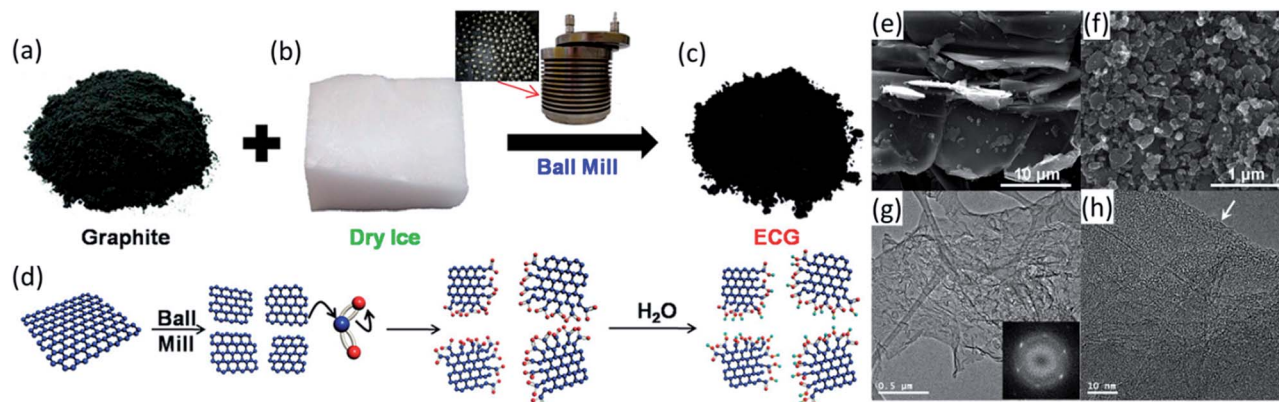


Fig. 15 (a) Pristine graphite. (b) Dry ice. (c) Edge-carboxylated graphite prepared by ball milling for 48 h. (d) A schematic representation of physical cracking and edge-carboxylation of graphite by ball milling in the presence of dry ice, and protonation through subsequent exposure to air moisture. SEM images of (e) the pristine graphite and (f) edge-carboxylated graphite. (g) TEM images of edge-carboxylated graphite at a low magnification. The inset shows a selected area electron diffraction pattern, showing high crystallinity. (h) Edge-on view of (g) at a higher magnification. Reproduced with permission from ref. 87. Copyright 2012 PNAS.

sonication and ball milling, rendering it as a potentially efficient technique for the scalable production of graphene. The fluid dynamics can be either mild or intensive.

**3.4.1 Vortex fluidic film.** By using a vortex fluidic film in a rapidly rotating tube (Fig. 16a), a less energy intensive shearing process for exfoliating graphite in an organic solvent<sup>99</sup> or water<sup>101</sup> is developed. The exfoliation mechanism lies in the partial lifting and slippage on the tube wall, as shown in Fig. 16b and c. The slippage process can be highlighted by the “finger print” of partially stacked graphene in Fig. 16d. This slippage process requires individual sheets to be partially lifted from the surface of the bulk material at some point to provide the necessary lateral force to start the slippage (Fig. 16b). Meanwhile, the graphite flakes are pushed against the tube wall by centrifugal force and experience a shear induced displacement along the tube, resulting in exfoliation at the tube surface (Fig. 16c). This vortex fluidic technique offers an alternative and tunable low-energy source for mild exfoliation and thus high-quality graphene. But the vortex fluidic film is extremely thin, which limits the quantity of graphite used for the exfoliation and the graphene output.

**3.4.2 Pressure driven fluid dynamics.** Contrastingly, in order to achieve large-scale production, based on high-pressure fluid dynamics, Shen *et al.* firstly reported the concept of jet

cavitation and designed a device for producing graphene.<sup>102–104</sup> But the involved mechanism and how to get high-concentration graphene were not well addressed. Subsequent deep investigation of the pressure driven fluid dynamics in micro channels has laid down the foundation for the scalable production of graphene and its analogues by fluid dynamics.<sup>97,98,100,105</sup> Two typical devices for high-pressure driven fluid dynamics are presented in Fig. 17a and b. The mixture of graphite and solvents is pressurized into the channel. The fluid dynamics happening in the channel are responsible for the exfoliation. In contrast to the sonication which is a normal-force-dominated way and the newly explored ball milling and fluidic film methods which are shear-force-dominated ways, pressure driven fluid dynamics has combined these two mechanisms and could achieve a much higher exfoliation efficiency.<sup>98,105</sup> Simulation analyses of the flow channel indicate that the high-pressure fluid dynamics route features cavitation, pressure release, viscous shear stress, turbulence, and collision. As shown in Fig. 17c, multiple fluid dynamics events are responsible for the normal-force dominated exfoliation and the shear-force dominated exfoliation. Cavitation and pressure release can generate a normal force for exfoliation. Velocity gradient-induced viscous shear stress, turbulence-induced Reynolds shear stress, and shear effects stemmed from turbulence and flow channel-induced collisions can generate shear force for exfoliation, resulting in the self-exfoliation of these bulk layered materials down to a single or few layers through their lateral self-lubricating ability.<sup>98,105</sup> The SEM image of the loose and transparent graphene flakes in Fig. 17e and the AFM image in Fig. 17f show the as-produced graphene. Most interestingly, if the pressure is significantly increased, the high-pressure fluid dynamics can be used to produce graphene nanomesh.<sup>100</sup> The mechanism is the combination of exfoliation and perforation of the graphene flakes (Fig. 18a). The obtained graphene nanomesh is shown in Fig. 18b and c. It is estimated that the total area of the pores within  $1 \mu\text{m}^2$  of nanomesh is  $\sim 0.15 \mu\text{m}^2$  and the pore density is  $\sim 22 \mu\text{m}^{-2}$ . This provides a novel route for the

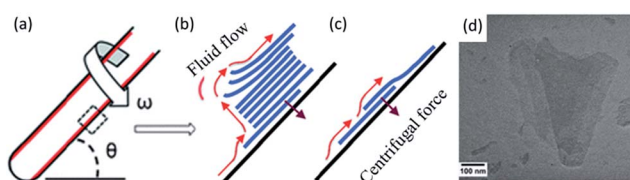


Fig. 16 (a) Schematic of the vortex fluidic device. (b) The exfoliation process with slippage and partial lift. (c) Slippage on the inner surface of the tube. (d) Partially stacked graphene for the evidence of slippage. Reproduced with permission from ref. 99. Copyright 2012 The Royal Society of Chemistry.

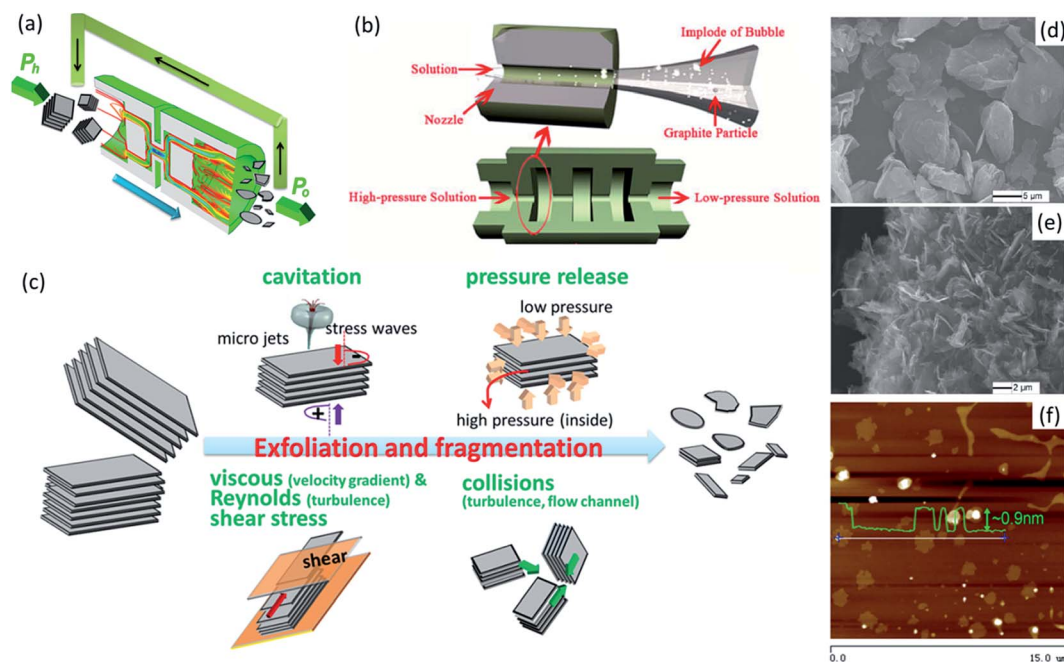


Fig. 17 (a) Schematic of the apparatus with one constriction channel for producing graphene. High pressure ( $P_h$ ) is exerted by a plunger pump and  $P_o$  denotes ambient pressure. (b) Schematic of the apparatus with four constriction channels. (c) Schematic of the exfoliation mechanism of the pressure driven fluid dynamics. SEM images of (d) graphite particles and (e) graphene flakes produced by the apparatus in (b). (f) AFM image of the graphene flakes prepared by the apparatus in (a). Reproduced with permission from ref. 97 and 98. Copyright 2013 and 2014 Springer.

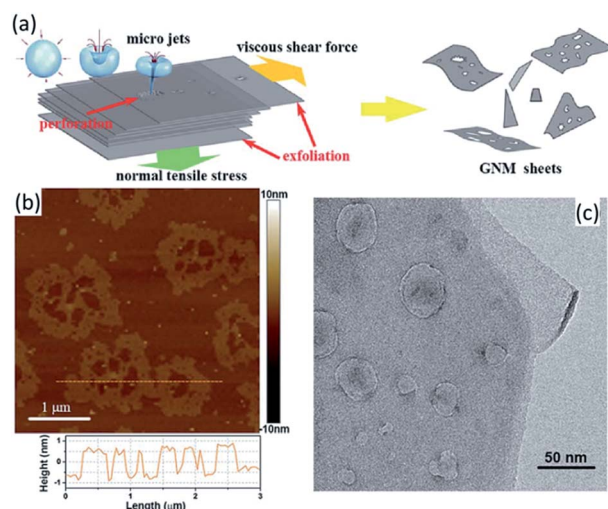


Fig. 18 (a) A schematic illustration for the pressure driven fluid dynamics for preparing graphene nanomesh. Typical (b) AFM and (c) TEM images of as-produced graphene nanomesh. Reproduced with permission from ref. 100. Copyright 2014 The Royal Society of Chemistry.

large-scale production of graphene nanomesh, which has been recently thought of as a new graphene-based nanostructure with suitable band gaps for the application of field-effect transistors.<sup>106,107</sup>

**3.4.3 Mixer driven fluid dynamics.** Another recently emerging method uses mixer driven fluid dynamics. The device for realizing this method is relatively simple and easily

available. Based on a high-shear rotor-stator mixer, Paton *et al.*<sup>108</sup> and Liu *et al.*<sup>109</sup> demonstrated a shear-assisted large-scale exfoliation for producing dispersions of graphene flakes. The apparatus used by them is shown in Fig. 19a–c, with a mixing head constituting a rotor and a stator as the critical components for exfoliation. The rotor diameters (Fig. 19b and c)

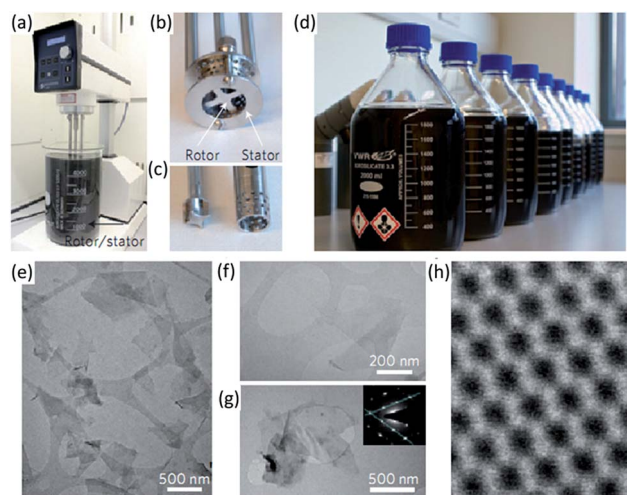


Fig. 19 (a) A Silverson model L5M high-shear mixer with mixing head in a 5 L beaker of graphene dispersion. (b) and (c) Mixing head with rotor and stator. (d) Graphene-NMP dispersions produced by shear exfoliation. (e)–(g) Wide-field TEM images of graphene nanosheets. (h) High-resolution TEM image of a monolayer. Reproduced with permission from ref. 108. Copyright 2014 Nature Publishing Group.



can be adjusted. The graphene flakes in the graphene–NMP dispersions (Fig. 19d) had lateral sizes of 300–800 nm, as measured by TEM and shown in the images in Fig. 19e and f. Based on the electron diffraction pattern, a multilayer (bottom left of Fig. 19g) and monolayer product (right of Fig. 19g) can also be ascertained.<sup>108</sup> The shear exfoliation mechanism was further revealed in terms of the rotor diameter and the characteristics of mixer-induced fluid dynamics. It was found that even when the Reynolds number  $Re_{\text{Mixer}}$  of the flow field is less than  $10^4$ , which corresponds to a not fully developed turbulent flow, well-exfoliated graphene still can be obtained, as shown in the region below the  $Re_{\text{Mixer}}$  line in Fig. 20a. But when the shear rate  $\dot{\gamma}$  is lower than  $10^4 \text{ s}^{-1}$ , graphite flakes are poorly exfoliated, as shown the region below the  $\dot{\gamma} = 10^4 \text{ s}^{-1}$  line in Fig. 20a. In the case of  $Re_{\text{Mixer}} < 10^4$ , *i.e.* laminar flow, graphene can still be well produced (Fig. 20b) if  $\dot{\gamma} > 10^4 \text{ s}^{-1}$ . In the case of shear mixing at a number of different combinations of rotating speed  $N$  and rotator diameter  $D$ , the minimum shear rate  $\dot{\gamma}_{\text{min}}$  is also around  $10^4 \text{ s}^{-1}$  (Fig. 20c). This suggests that any mixer that can achieve a shear rate above  $10^4 \text{ s}^{-1}$  can be used to produce graphene. The exfoliation mechanism that occurs in both laminar and turbulent regimes should be the same, and good exfoliation can happen without turbulence.<sup>108</sup> Further, Liu *et al.*<sup>109</sup> qualitatively explained the exfoliation mechanism in terms of fluid dynamics events, as illustrated in Fig. 21. Like ball milling and vortex fluidics, this is a shear-force dominated method. But cavitation and collision effects also favor efficient exfoliation, as shown in Fig. 21. However, in the rotor-stator mixer (Fig. 19b and c), very high shear rates are mainly localized in the gap between the rotor and stator and in the holes in the stator. This implies a well-defined localized region of high shear rate, indicating that

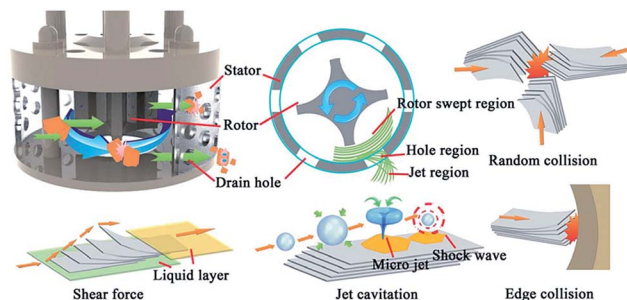


Fig. 21 3D sectional drawing of the high-shear mixer, and the schematic mechanical mechanism for preparing graphene by shear force, collision, and cavitation. Reproduced with permission from ref. 109. Copyright 2014 The Royal Society of Chemistry.

most of the exfoliation events are localized in the vicinity of the rotor-stator.

In order to overcome the shortcomings of the rotor-stator mixer, a full developed turbulence with all the regions of high shear rate is necessary. Initially, Alhassan *et al.* used a stainless steel blender equipped with a four-blade impeller to generate turbulence, and demonstrated the feasibility of graphite exfoliation by turbulent mixing.<sup>110</sup> But they only focused on this arresting concept using laponite, they did not go further in their comprehensive optimization to achieve predominantly monolayer graphene. Recently, Yi *et al.*<sup>111,112</sup> and Varla *et al.*<sup>113</sup> have promoted this technique. They used a kitchen blender to generate a full turbulent flow for graphene production, as shown in Fig. 22. In a kitchen blender, a simple and easily available rotating-blade mixer, the high-shear region is not localized in any single portion of the holder. Though the shear rate decreases with the increasing distance from the blade, the high shear rate can cover all of the holder if turbulence is fully developed. Therefore, the turbulence is mainly responsible for the full-field high shear rate and thus the exfoliation mechanism, as shown in Fig. 22b. In terms of the characteristics of the turbulent flow in the kitchen blender, it is demonstrated that four fluid dynamics events are responsible for the exfoliation and fragmentation: (I) the velocity gradient can induce viscous shear stress; (II) intensive velocity fluctuations in the turbulence can induce Reynolds shear stress; (III) in the turbulence, the Reynolds number is very large, and thus the inertial forces dominate the viscous forces to enhance graphite–graphite collisions; (IV) it is possible that a turbulent pressure fluctuation induced pressure difference can also exfoliate graphite in a normal-force style. The mechanism can be verified from TEM observations. The slipped configuration with lateral relative displacement of translation (Fig. 22c) or rotation (Fig. 22d) indicates that lateral exfoliation really happens and two ways coexist, *i.e.* translation and rotation. The exfoliation efficiency is much higher than that in standard sonication or ball milling exfoliation methods. These results imply that industrial rotating blade stirred tank reactors are a promising new technology for large-scale graphene production.

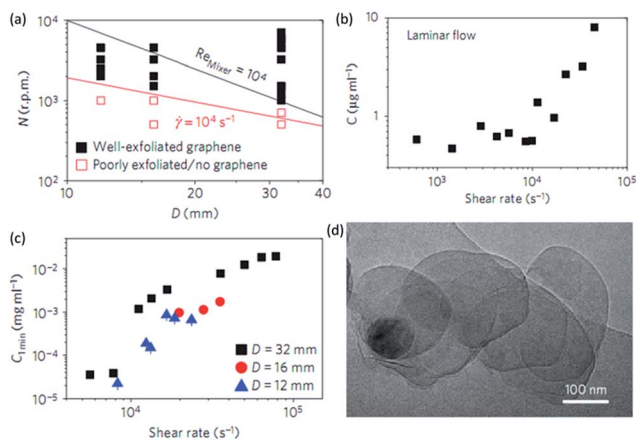


Fig. 20 (a) Phase diagram of rotor speed,  $N$ , versus the mixing head diameter,  $D$ , for dispersions showing good exfoliation. The region above the black line represents fully developed turbulence, that is,  $Re_{\text{Mixer}} > 10^4$ , whereas the region above the red line represents  $\dot{\gamma}_{\text{min}} > 10^4 \text{ s}^{-1}$ . (b) Concentration of graphene as a function of shear rate (mixing time 60 min). (c) Concentration of graphene as a function of shear rate for rotors with diameters of 32, 16 and 12 mm (mixing time 1 min). All of the three data sets are consistent with the same minimum shear rate. (d) TEM image of a partially exfoliated BN flake, consistent with exfoliation by shear sliding. Reproduced with permission from ref. 108. Copyright 2014 Nature Publishing Group.



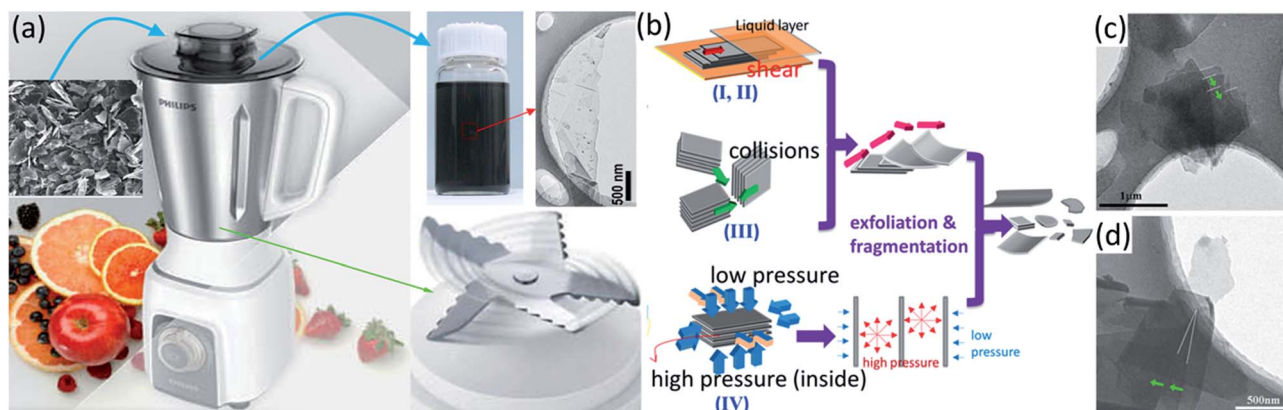


Fig. 22 (a) The schematic of a kitchen blender used for preparing graphene flakes. (b) Illustration of the exfoliation mechanism. Deliberately captured partially exfoliated graphene flakes with translational (c) and rotational (d) lateral exfoliation. Reproduced with permission from ref. 112. Copyright 2014 Elsevier.

The fluid dynamics method has already been discovered to be ambitious for generating FLG solutions. When compared to localized and high-energy cavitation-dominated sonication or shear-dominated ball milling, fluid dynamics can carry graphite particles all over the flow field and multiple fluid dynamics events are favourable for mild and efficient exfoliation. Nevertheless, detailed studies are still needed to proceed from discovery to a commercialized technology. In the high-shear mixer or kitchen blender, intensive cavitation can happen around the rotor/stator or rotating blade, resulting in possible defects. The exhaustive and precise design of the fluid dynamics to achieve mild and efficient exfoliation throughout the flow field, eliminate the localized region, and minimize the cavitation effects is necessary for industrial scale up.

### 3.5 Other methods

The last two mechanical methods though less intensively investigated should be mentioned. The first one is the detonation technique for preparing graphene materials.<sup>114,115</sup> It relies on the detonation induced powerful shockwave and thermal energy for high-energy and violent exfoliation. Though it is extremely efficient, graphite oxide was often used as the precursor and graphene oxide rather than pristine graphene was produced.<sup>114,115</sup> So far, there have been no reports about the detonation assisted production of pristine graphene. The second one is exfoliation assisted by a supercritical fluid.<sup>115–119</sup> It depends on the high diffusivity, expansibility, and solvating power of the supercritical fluid. The supercritical fluid can penetrate into the gap between the graphite layers. Once a rapid depressurization happens, the supercritical fluid will abruptly expand to predominately generate a normal force for exfoliating graphite. For example, Pu *et al.*<sup>115</sup> reported graphene flakes obtained by discharging expanding CO<sub>2</sub> gas into a solution containing a sodium dodecyl sulfate dispersant, and the typical graphene flake contained about 10 atomic layers. Lately, Rangappa *et al.*<sup>116</sup> extended the idea of using a supercritical fluid. They utilized a supercritical fluid of ethanol, NMP, and DMF to directly

exfoliate graphite crystals into graphene flakes, as shown in Fig. 23. They heated the solvents up to or above their critical temperature. With a low interfacial tension, excellent wetting of surfaces, and high diffusion coefficients, these supercritical fluids can rapidly penetrate into the interlayers of graphite with a high solvation power. The exfoliation of graphite down to a few layers (<10 layers) can be achieved in the shortest reaction time of 15 min. About 90–95% of the exfoliated sheets are less than 8 layers with approximately 6–10% monolayers.<sup>116</sup> Combining the functionalization of graphene, Zheng *et al.*<sup>118</sup> and Li *et al.*<sup>117</sup> prepared graphene in pyrene and its derivatives with the assistance of supercritical CO<sub>2</sub>, as illustrated in Fig. 24. This method established the use of a supercritical fluid as an alternative route for the high-throughput production and functionalization of graphene in one step. Recently, the combination of supercritical fluid and sonication was also reported by Gao *et al.*<sup>119</sup> They demonstrated that the obtained graphene flakes are 24% monolayers, 44% bilayers, and 26% trilayers. These results are very intriguing in terms of the graphene layer number. If supercritical fluid processing can be made easy and the use of a pressurized reactor can be avoided, supercritical fluid techniques are very promising for the facile and scalable production of high quality graphene.

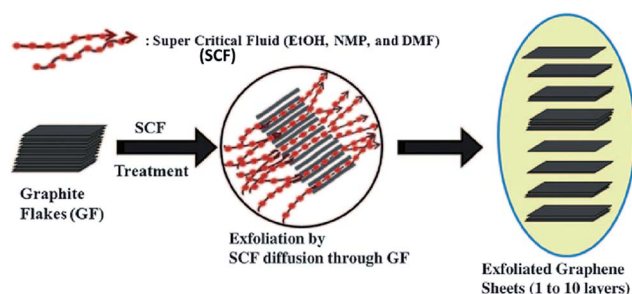


Fig. 23 Scheme showing the exfoliation of graphite crystals to graphene using a supercritical fluid such as ethanol (EtOH), NMP, and DMF. Reproduced with permission from ref. 116. Copyright 2010 Wiley-VCH.

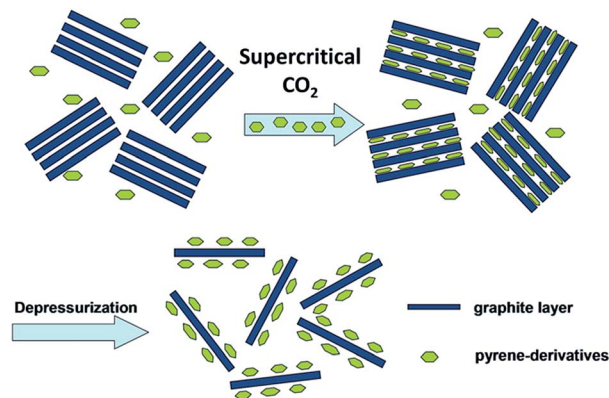


Fig. 24 Schematic for the exfoliation and modification of graphene by pyrene-derivatives with the assistance of supercritical carbon dioxide. Reproduced with permission from ref. 117. Copyright 2013 American Chemical Society.

## 4. Conclusions and outlook

The mechanical exfoliation of graphite to give graphene has been a promising approach for the scalable production of graphene. Although different techniques or apparatus have been utilized to produce graphene, the mechanical mechanism involved in the exfoliation is similar, *i.e.* generating a shear force or a normal force. From the viewpoint of mechanics, the core task is to mechanically overcome the van der Waals attractions between the graphene layers within the bulk precursor. Once exfoliation has happened, chemistry should play a critical role which is beyond the scope here.

In this review, we have discussed several mechanical exfoliation methods, such as using micromechanical cleavage, sonication, ball milling, fluid dynamics, supercritical fluids, *etc.* All of these methods have been widely demonstrated to have the ability to produce graphene. Some of them are also commercialized techniques which have been widely used in traditional industry. Sonication is a cavitation-dominated technique. It leads to a normal-force dominated exfoliation and cavitation-induced harsh local environment. Ball milling features shear force, as well as a high energy output for functionalization. The pressure driven fluid dynamics method combines the advantages of sonication and ball milling. It generates multiple fluid dynamic events for efficient exfoliation. Mixer driven fluid dynamics methods depend on high local shear rates or turbulence for exfoliation. For methods using a supercritical fluid, penetration into the layer gap and depressurizing induced abrupt expansion lead to a normal-force dominated exfoliation.

In spite of the vital prospect of mechanical exfoliation, several issues still require continuous attention. Although substantial efforts have been made to improve the yield and degree of exfoliation through the above mechanical techniques, the yield of monolayer graphene is still quite low. Moreover, a large majority of graphite is not exfoliated and centrifugation is needed. So it is very important in the near future to enhance the mechanical exfoliation efficiency. All of the mechanical exfoliation techniques have fragmentation effects which are not

desired for producing large-size graphene. How to minimize the fragmentation effects should be considered. For sonication, technical factors, such as power, frequency, vessel geometry, sonication source distribution, *etc.*, should attract interest for optimizing the exfoliation efficiency and scaling up production. For the ball milling method, the type, size, and rotation speed of the grinding media and how to precisely control high-energy collisions are very important. For the fluid dynamics method, a deep understanding and careful design of the flow field are critical for eliminating the localized region and achieving high shear rates throughout the flow field. For the supercritical fluid method, it will be much better if a facile device or related technology is easily available and the production cost is lowered. Though there have been some reports on cavitation induced defects in graphene produced by sonication, little information about the defects induced by other mechanical exfoliation techniques is available. Future challenges should also focus on problems such as uncontrollable defects, random size, and the random layer number of graphene produced using mechanical exfoliation methods.

## Acknowledgements

The authors acknowledge financial support by the Beijing Natural Science Foundation (2132025), Specialized Research Fund for the Doctoral Program of Higher Education (20131102110016), the Innovation Foundation of BUAA for PhD Graduates (YWF-14-YJSY-052), and the China Scholarship Council (CSC).

## Notes and references

- 1 K. S. Novoselov, A. K. Geim, S. V. Morozov, D. Jiang, Y. Zhang, S. V. Dubonos, I. V. Grigorieva and A. A. Firsov, *Science*, 2004, **306**, 666–669.
- 2 K. S. Novoselov, D. Jiang, F. Schedin, T. J. Booth, V. V. Khotkevich, S. V. Morozov and A. K. Geim, *Proc. Natl. Acad. Sci. U. S. A.*, 2005, **102**, 10451–10453.
- 3 A. K. Geim and K. S. Novoselov, *Nat. Mater.*, 2007, **6**, 183–191.
- 4 A. K. Geim, *Science*, 2009, **324**, 1530–1534.
- 5 M. J. Allen, V. C. Tung and R. B. Kaner, *Chem. Rev.*, 2010, **110**, 132–145.
- 6 K. S. Novoselov, V. I. Fal'ko, L. Colombo, P. R. Gellert, M. G. Schwab and K. Kim, *Nature*, 2012, **490**, 192–200.
- 7 E. P. Randviir, D. A. C. Brownson and C. E. Banks, *Mater. Today*, 2014, **17**, 426–432.
- 8 K. S. Novoselov, A. K. Geim, S. V. Morozov, D. Jiang, M. I. Katsnelson, I. V. Grigorieva, S. V. Dubonos and A. A. Firsov, *Nature*, 2005, **438**, 197–200.
- 9 A. S. Mayorov, R. V. Gorbachev, S. V. Morozov, L. Britnell, R. Jalil, L. A. Ponomarenko, P. Blake, K. S. Novoselov, K. Watanabe, T. Taniguchi and A. K. Geim, *Nano Lett.*, 2011, **11**, 2396–2399.
- 10 J. Moser, A. Barreiro and A. Bachtold, *Appl. Phys. Lett.*, 2007, **91**, 163513.

- 11 C. Lee, X. Wei, J. W. Kysar and J. Hone, *Science*, 2008, **321**, 385–388.
- 12 F. Liu, P. Ming and J. Li, *Phys. Rev. B: Condens. Matter Mater. Phys.*, 2007, **76**, 064120.
- 13 A. A. Balandin, *Nat. Mater.*, 2011, **10**, 569–581.
- 14 A. A. Balandin, S. Ghosh, W. Bao, I. Calizo, D. Teweldebrhan, F. Miao and C. N. Lau, *Nano Lett.*, 2008, **8**, 902–907.
- 15 J. S. Bunch, S. S. Verbridge, J. S. Alden, A. M. van der Zande, J. M. Parpia, H. G. Craighead and P. L. McEuen, *Nano Lett.*, 2008, **8**, 2458–2462.
- 16 R. R. Nair, P. Blake, A. N. Grigorenko, K. S. Novoselov, T. J. Booth, T. Stauber, N. M. Peres and A. K. Geim, *Science*, 2008, **320**, 1308.
- 17 Y. Zhang, L. Zhang and C. Zhou, *Acc. Chem. Res.*, 2013, **46**, 2329–2339.
- 18 X. Li, W. Cai, J. An, S. Kim, J. Nah, D. Yang, R. Piner, A. Velamakanni, I. Jung, E. Tutuc, S. K. Banerjee, L. Colombo and R. S. Ruoff, *Science*, 2009, **324**, 1312–1314.
- 19 C. Berger, Z. Song, T. Li, X. Li, A. Y. Ogbazghi, R. Feng, Z. Dai, A. N. Marchenkov, E. H. Conrad, P. N. First and W. A. de Heer, *J. Phys. Chem. B*, 2004, **108**, 19912–19916.
- 20 C. Mattevi, H. Kim and M. Chhowalla, *J. Mater. Chem.*, 2011, **21**, 3324.
- 21 W. Strupinski, K. Grodecki, A. Wysmolek, R. Stepniewski, T. Szkopek, P. E. Gaskell, A. Gruneis, D. Haberer, R. Bozek, J. Krupka and J. M. Baranowski, *Nano Lett.*, 2011, **11**, 1786–1791.
- 22 H. Ago, Y. Ito, N. Mizuta, K. Yoshida, B. Hu, C. M. Orofeo, M. Tsuji, K. Ikeda and S. Mizuno, *ACS Nano*, 2010, **4**, 7407–7414.
- 23 H. K. Yu, K. Balasubramanian, K. Kim, J. L. Lee, M. Maiti, C. Ropers, J. Krieg, K. Kern and A. M. Wodtke, *ACS Nano*, 2014, **8**, 8636–8643.
- 24 B. Hu, H. Ago, Y. Ito, K. Kawahara, M. Tsuji, E. Magome, K. Sumitani, N. Mizuta, K.-i. Ikeda and S. Mizuno, *Carbon*, 2012, **50**, 57–65.
- 25 C. Vo-Van, A. Kimouche, A. Reserbat-Plantey, O. Fruchart, P. Bayle-Guillemaud, N. Bendiab and J. Coraux, *Appl. Phys. Lett.*, 2011, **98**, 181903.
- 26 J. N. Coleman, *Adv. Funct. Mater.*, 2009, **19**, 3680–3695.
- 27 J. N. Coleman, *Acc. Chem. Res.*, 2013, **46**, 14–22.
- 28 X. Cui, C. Zhang, R. Hao and Y. Hou, *Nanoscale*, 2011, **3**, 2118–2126.
- 29 Y. Hernandez, V. Nicolosi, M. Lotya, F. M. Blighe, Z. Sun, S. De, I. T. McGovern, B. Holland, M. Byrne, Y. K. Gun'ko, J. J. Boland, P. Niraj, G. Duesberg, S. Krishnamurthy, R. Goodhue, J. Hutchison, V. Scardaci, A. C. Ferrari and J. N. Coleman, *Nat. Nanotechnol.*, 2008, **3**, 563–568.
- 30 A. Ciesielski and P. Samori, *Chem. Soc. Rev.*, 2014, **43**, 381–398.
- 31 W. Du, X. Jiang and L. Zhu, *J. Mater. Chem. A*, 2013, **1**, 10592.
- 32 Y. L. Zhong, Z. Tian, G. P. Simon and D. Li, *Mater. Today*, 2015, **18**, 73–78.
- 33 D. R. Dreyer, S. Park, C. W. Bielawski and R. S. Ruoff, *Chem. Soc. Rev.*, 2010, **39**, 228–240.
- 34 K. P. Loh, Q. Bao, P. K. Ang and J. Yang, *J. Mater. Chem.*, 2010, **20**, 2277–2289.
- 35 M. Cai, D. Thorpe, D. H. Adamson and H. C. Schniepp, *J. Mater. Chem.*, 2012, **22**, 24992.
- 36 Y. Hernandez, M. Lotya, D. Rickard, S. D. Bergin and J. N. Coleman, *Langmuir*, 2010, **26**, 3208–3213.
- 37 M. Yi, Z. Shen, S. Ma and X. Zhang, *J. Nanopart. Res.*, 2012, **14**, 1003.
- 38 M. Yi, Z. Shen, X. Zhang and S. Ma, *J. Phys. D: Appl. Phys.*, 2013, **46**, 025301.
- 39 M. Lotya, Y. Hernandez, P. J. King, R. J. Smith, V. Nicolosi, L. S. Karlsson, F. M. Blighe, S. De, Z. Wang, I. T. McGovern, G. S. Duesberg and J. N. Coleman, *J. Am. Chem. Soc.*, 2009, **131**, 3611–3620.
- 40 M. Lotya, P. J. King, U. Khan, S. De and J. N. Coleman, *ACS Nano*, 2010, **4**, 3155–3162.
- 41 L. Guardia, M. J. Fernández-Merino, J. I. Paredes, P. Solís-Fernández, S. Villar-Rodil, A. Martínez-Alonso and J. M. D. Tascón, *Carbon*, 2011, **49**, 1653–1662.
- 42 S. Vadukumpully, J. Paul and S. Valiyaveetil, *Carbon*, 2009, **47**, 3288–3294.
- 43 A. B. Bourlinos, V. Georgakilas, R. Zboril, T. A. Steriotis and A. K. Stubos, *Small*, 2009, **5**, 1841–1845.
- 44 D. Nuvoli, L. Valentini, V. Alzari, S. Scognamiglio, S. B. Bon, M. Piccinini, J. Illescas and A. Mariani, *J. Mater. Chem.*, 2011, **21**, 3428.
- 45 X. Zhou, T. Wu, K. Ding, B. Hu, M. Hou and B. Han, *Chem. Commun.*, 2010, **46**, 386–388.
- 46 M. S. Dresselhaus and P. T. Araujo, *ACS Nano*, 2010, **4**, 6297–6302.
- 47 B. Jayasena and S. Subbiah, *Nanoscale Res. Lett.*, 2011, **6**, 95.
- 48 J. Chen, M. Duan and G. Chen, *J. Mater. Chem.*, 2012, **22**, 19625.
- 49 A. B. Bourlinos, V. Georgakilas, R. Zboril, T. A. Steriotis, A. K. Stubos and C. Trapalis, *Solid State Commun.*, 2009, **149**, 2172–2176.
- 50 A. O'Neill, U. Khan, P. N. Nirmalraj, J. Boland and J. N. Coleman, *J. Phys. Chem. C*, 2011, **115**, 5422–5428.
- 51 Y.-T. Liu, X.-M. Xie and X.-Y. Ye, *Carbon*, 2011, **49**, 3529–3537.
- 52 U. Khan, A. O'Neill, M. Lotya, S. De and J. N. Coleman, *Small*, 2010, **6**, 864–871.
- 53 A. S. Wajid, S. Das, F. Irin, H. S. T. Ahmed, J. L. Shelburne, D. Parviz, R. J. Fullerton, A. F. Jankowski, R. C. Hedden and M. J. Green, *Carbon*, 2012, **50**, 526–534.
- 54 U. Khan, H. Porwal, A. O'Neill, K. Nawaz, P. May and J. N. Coleman, *Langmuir*, 2011, **27**, 9077–9082.
- 55 S. M. Notley, *Langmuir*, 2012, **28**, 14110–14113.
- 56 L. Xu, J.-W. McGraw, F. Gao, M. Grundy, Z. Ye, Z. Gu and J. L. Shepherd, *J. Phys. Chem. C*, 2013, **117**, 10730–10742.
- 57 S. Wang, M. Yi, Z. Shen, X. Zhang and S. Ma, *RSC Adv.*, 2014, **4**, 25374.
- 58 J.-W. T. Seo, A. A. Green, A. L. Antaris and M. C. Hersam, *J. Phys. Chem. Lett.*, 2011, **2**, 1004–1008.
- 59 Z. Sun, J. Vivekananthan, D. A. Guschin, X. Huang, V. Kuznetsov, P. Ebbinghaus, A. Sarfraz, M. Muhler and W. Schuhmann, *Chemistry*, 2014, **20**, 5752–5761.



- 60 J. Li, F. Ye, S. Vaziri, M. Muhammed, M. C. Lemme and M. Östling, *Carbon*, 2012, **50**, 3113–3116.
- 61 X. Zhang, A. C. Coleman, N. Katsonis, W. R. Browne, B. J. van Wees and B. L. Feringa, *Chem. Commun.*, 2010, **46**, 7539–7541.
- 62 U. Khan, A. O'Neill, H. Porwal, P. May, K. Nawaz and J. N. Coleman, *Carbon*, 2012, **50**, 470–475.
- 63 M. Lotya, A. Rakovich, J. F. Donegan and J. N. Coleman, *Nanotechnology*, 2013, **24**, 265703.
- 64 L. Lin, X. Zheng, S. Zhang and D. A. Allwood, *Adv. Mater. Interfaces*, 2014, **1**, 1300078.
- 65 G. Cravotto and P. Cintas, *Chem.–Eur. J.*, 2010, **16**, 5246–5259.
- 66 M. V. Bracamonte, G. I. Lacconi, S. E. Urreta and L. E. F. Foa Torres, *J. Phys. Chem. C*, 2014, **118**, 15455–15459.
- 67 T. Skaltsas, X. Ke, C. Bittencourt and N. Tagmatarchis, *J. Phys. Chem. C*, 2013, **117**, 23272–23278.
- 68 M. Yi, Z. Shen, S. Liang, L. Liu, X. Zhang and S. Ma, *Chem. Commun.*, 2013, **49**, 11059–11061.
- 69 E. Y. Polyakova Stolyarova, K. T. Rim, D. Eom, K. Douglass, R. L. Opila, T. F. Heinz, A. V. Teplyakov and G. W. Flynn, *ACS Nano*, 2011, **5**, 6102–6108.
- 70 E. B. Flint and K. S. Suslick, *Science*, 1991, **253**, 1397–1399.
- 71 K. S. Suslick, W. B. McNamara and Y. T. Didenko, *Nature*, 1999, **401**, 772–775.
- 72 K. S. Suslick and D. J. Flannigan, *Annu. Rev. Phys. Chem.*, 2008, **59**, 659–683.
- 73 M. Yi, Z. Shen, X. Zhang and S. Ma, *J. Mater. Sci.*, 2012, **47**, 8234–8244.
- 74 V. S. Sutkar and P. R. Gogate, *Chem. Eng. J.*, 2009, **155**, 26–36.
- 75 B. Nanzai, K. Okitsu, N. Takenaka, H. Bandow, N. Tajima and Y. Maeda, *Ultrason. Sonochem.*, 2009, **16**, 163–168.
- 76 Y. Kojima, S. Koda and H. Nomura, *Jpn. J. Appl. Phys.*, 1998, **37**, 2992–2995.
- 77 Y. Asakura, T. Nishida, T. Matsuoka and S. Koda, *Ultrason. Sonochem.*, 2008, **15**, 244–250.
- 78 J. T. Han, J. I. Jang, H. Kim, J. Y. Hwang, H. K. Yoo, J. S. Woo, S. Choi, H. Y. Kim, H. J. Jeong, S. Y. Jeong, K. J. Baeg, K. Cho and G. W. Lee, *Sci. Rep.*, 2014, **4**, 5133.
- 79 A. E. Del Rio-Castillo, C. Merino, E. Díez-Barra and E. Vázquez, *Nano Res.*, 2014, **7**, 963–972.
- 80 C. Damm, T. J. Nacken and W. Peukert, *Carbon*, 2015, **81**, 284–294.
- 81 M. Antisari, A. Montone, N. Jovic, E. Piscopiello, C. Alvani and L. Piloni, *Scr. Mater.*, 2006, **55**, 1047–1050.
- 82 A. Milev, M. Wilson, G. S. K. Kannangara and N. Tran, *Mater. Chem. Phys.*, 2008, **111**, 346–350.
- 83 R. Janot and D. Guérard, *Carbon*, 2002, **40**, 2887–2896.
- 84 C. Knieke, A. Berger, M. Voigt, R. N. K. Taylor, J. Röhl and W. Peukert, *Carbon*, 2010, **48**, 3196–3204.
- 85 W. Zhao, M. Fang, F. Wu, H. Wu, L. Wang and G. Chen, *J. Mater. Chem.*, 2010, **20**, 5817.
- 86 W. Zhao, F. Wu, H. Wu and G. Chen, *J. Nanomater.*, 2010, **2010**, 1–5.
- 87 I. Y. Jeon, Y. R. Shin, G. J. Sohn, H. J. Choi, S. Y. Bae, J. Mahmood, S. M. Jung, J. M. Seo, M. J. Kim, D. Wook Chang, L. Dai and J. B. Baek, *Proc. Natl. Acad. Sci. U. S. A.*, 2012, **109**, 5588–5593.
- 88 Y. Yao, Z. Lin, Z. Li, X. Song, K.-S. Moon and C.-p. Wong, *J. Mater. Chem.*, 2012, **22**, 13494.
- 89 R. Aparna, N. Sivakumar, A. Balakrishnan, A. Sreekumar Nair, S. V. Nair and K. R. V. Subramanian, *J. Renewable Sustainable Energy*, 2013, **5**, 033123.
- 90 I. Y. Jeon, H. J. Choi, S. M. Jung, J. M. Seo, M. J. Kim, L. Dai and J. B. Baek, *J. Am. Chem. Soc.*, 2013, **135**, 1386–1393.
- 91 J. H. Lee, *Int. J. Mater. Sci. Appl.*, 2013, **2**, 209.
- 92 O. Y. Posudievsky, O. A. Khazieieva, V. V. Cherepanov, V. G. Koshechko and V. D. Pokhodenko, *J. Nanopart. Res.*, 2013, **15**, 2046.
- 93 M. Borah, M. Dahiya, S. Sharma, R. B. Mathur and S. R. Dhakate, *Mater. Focus*, 2014, **3**, 300–309.
- 94 V. Leon, A. M. Rodriguez, P. Prieto, M. Prato and E. Vazquez, *ACS Nano*, 2014, **8**, 563–571.
- 95 Y. Lv, L. Yu, C. Jiang, S. Chen and Z. Nie, *RSC Adv.*, 2014, **4**, 13350.
- 96 T. Lin, Y. Tang, Y. Wang, H. Bi, Z. Liu, F. Huang, X. Xie and M. Jiang, *Energy Environ. Sci.*, 2013, **6**, 1283.
- 97 L. Liu, Z. Shen, S. Liang, M. Yi, X. Zhang and S. Ma, *J. Mater. Sci.*, 2013, **49**, 321–328.
- 98 M. Yi, Z. Shen and J. Zhu, *Chin. Sci. Bull.*, 2014, **59**, 1794–1799.
- 99 X. Chen, J. F. Dobson and C. L. Raston, *Chem. Commun.*, 2012, **48**, 3703–3705.
- 100 S. Liang, M. Yi, Z. Shen, L. Liu, X. Zhang and S. Ma, *RSC Adv.*, 2014, **4**, 16127.
- 101 M. H. Wahid, E. Eroglu, X. Chen, S. M. Smith and C. L. Raston, *Green Chem.*, 2013, **15**, 650.
- 102 Z. Shen, J. Li, M. Yi, X. Zhang and S. Ma, *Nanotechnology*, 2011, **22**, 365306.
- 103 M. Yi, J. Li, Z. Shen, X. Zhang and S. Ma, *Appl. Phys. Lett.*, 2011, **99**, 123112.
- 104 J. Li, M. Yi, Z. Shen, S. Ma, X. Zhang and Y. Xing, *Sci. China: Technol. Sci.*, 2012, **55**, 2815–2819.
- 105 M. Yi, Z. Shen, W. Zhang, J. Zhu, L. Liu, S. Liang, X. Zhang and S. Ma, *Nanoscale*, 2013, **5**, 10660–10667.
- 106 J. Bai, X. Zhong, S. Jiang, Y. Huang and X. Duan, *Nat. Nanotechnol.*, 2010, **5**, 190–194.
- 107 L. Jiang and Z. Fan, *Nanoscale*, 2014, **6**, 1922–1945.
- 108 K. R. Paton, E. Varrla, C. Backes, R. J. Smith, U. Khan, A. O'Neill, C. Boland, M. Lotya, O. M. Istrate, P. King, T. Higgins, S. Barwich, P. May, P. Puczkarski, I. Ahmed, M. Moebius, H. Pettersson, E. Long, J. Coelho, S. E. O'Brien, E. K. McGuire, B. M. Sanchez, G. S. Duesberg, N. McEvoy, T. J. Pennycook, C. Downing, A. Crossley, V. Nicolosi and J. N. Coleman, *Nat. Mater.*, 2014, **13**, 624–630.
- 109 L. Liu, Z. Shen, M. Yi, X. Zhang and S. Ma, *RSC Adv.*, 2014, **4**, 36464.
- 110 S. M. Alhassan, S. Qutubuddin and D. A. Schiraldi, *Langmuir*, 2012, **28**, 4009–4015.
- 111 Z. Shen, M. Yi, S. Ma and X. Zhang, *Turbulence method for preparing high-quality graphene*, China Pat., CN103350995A, 2013.

- 112 M. Yi and Z. Shen, *Carbon*, 2014, **78**, 622–626.
- 113 E. Varrla, K. R. Paton, C. Backes, A. Harvey, R. J. Smith, J. McCauley and J. N. Coleman, *Nanoscale*, 2014, **6**, 11810–11819.
- 114 G. Sun, X. Li, Y. Qu, X. Wang, H. Yan and Y. Zhang, *Mater. Lett.*, 2008, **62**, 703–706.
- 115 N.-W. Pu, C.-A. Wang, Y. Sung, Y.-M. Liu and M.-D. Ger, *Mater. Lett.*, 2009, **63**, 1987–1989.
- 116 D. Rangappa, K. Sone, M. Wang, U. K. Gautam, D. Golberg, H. Itoh, M. Ichihara and I. Honma, *Chem.–Eur. J.*, 2010, **16**, 6488–6494.
- 117 L. Li, X. Zheng, J. Wang, Q. Sun and Q. Xu, *ACS Sustainable Chem. Eng.*, 2013, **1**, 144–151.
- 118 X. Zheng, Q. Xu, J. Li, L. Li and J. Wei, *RSC Adv.*, 2012, **2**, 10632.
- 119 Y. Gao, W. Shi, W. Wang, Y. Wang, Y. Zhao, Z. Lei and R. Miao, *Ind. Eng. Chem. Res.*, 2014, **53**, 2839–2845.